Nanoscale infrared spectral imaging for non-invasive intracellular gold nanoparticle conjugate localization

Eamonn Kennedy[†], Rasoul Al-Majmaie[†§], Mohamed Al-Rubeai[§], Dominic Zerulla[†], James H Rice[†]*

[†]School of Physics, and [§]School of Chemical and Bioprocess Engineering, University College Dublin, Ireland

KEYWORDS: AFM, AFM-IR, Photothermal induced resonance, Cancer nanotechnology, Gold nanoparticles, nanoimaging.

ABSTRACT

This paper reports on the use of infrared (IR) nanospectral absorption imaging to map the subcellular localization of toluidine blue-conjugated gold nanoparticles within colon adenocarcinoma cells. The spatial and spectral accuracy of the IR imaging method is confirmed via co-localization of the nanoparticles on a cell by cell basis using conventional fluorescence microscopy. IR spectral ratio imaging is presented as a means to map intracellular nanoparticle density at sub 50 nm lateral resolution with IR nanospectroscopy enabling distinction of nanoparticle seeded cells from a control group with 95% confidence. In this way we illustrate

that IR absorption nanoimaging, combined with IR point source data permits extension of the AFM-IR technique from subcellular analysis up to studies of cell numbers that are statistically significant.

INTRODUCTION

Gold nanoparticles (GNPs) are attractive for a diverse range of applications in cellular biology and medicine due to their unique chemical and optical properties.[1] Their use has become prominent in cancer research due to their size-tunable preferential accumulation in cancer cells[2,3] which can be further enhanced by conjugation to molecules which promote cancer selective nanoparticle endocytosis. GNPs have resonant light scattering properties and high absorption cross sections per unit volume that can enhance local fluorescence and plasmonic signals, making them invaluable tools in low contrast biomolecular imaging.[4,5] However, effective use of nanoparticles as cell imaging agents requires quantitative information about how cells distribute the nanoparticles internally. This has led to extensive research on cellular uptake and the intracellular distribution of nanoparticles.[6]

GNPs can be imaged by labeling with fluorescence microscopy or by label free methods such as dark field contrast imaging.[7] However, conventional optical methods cannot image at the spatial resolution of nanoparticles themselves as they are diffraction limited. Additionally, fluorescent markers may be unattractive depending on cost and the potential for unwanted secondary chemical interactions within the cell. Therefore electron microscopy is an attractive choice for quantitative analysis of nanoparticle-cell experiments.[8] Such methods as transmission electron microscopy (TEM), which require pre-treatment with a microtome and staining can provide true nanoimaging, although they are limited by experimental considerations such as slice

orientation and blade or laser quality.[9] Critically, these methods are considered invasive as they destroy the cell in the slicing or staining process. This limitation has led to intense research on the application of non-destructive nanoscale resolution imaging methods.[10,11] One of the key motivations for the application of these methods is to provide is information on the distribution of nanoparticles that carry covalently linked drugs on their surface which can exhibit significant enhancement of the singlet oxygen quantum yield as compared with free photosensitizers.[12] It is evident that greater understanding of intracellular nanoparticle distribution through localization methodologies has the potential to increase uptake and the selectivity of targeted delivery in nanotherapy. However, such understanding of the processes underlying sensitizing nanomaterials in cells requires methods that are not only high resolution, but are also chemically specific to the sensitizer.

Methods to enhance the resolution of conventional optical methods to the nanoscale include stimulated emission depletion microscopy (STED)[13] and Raman based, tip enhanced methods such as TERS[14] or the exploitation of nonlinear optical processes such as coherent anti-stokes raman spectroscopy (CARS)[15] which have both previously been used for nanoscale resolution chemical discrimination within biological media. In contrast, conventional IR absorption imaging is far more limited by diffraction than visible light source methods since resolution scales with wavelength.[16] This restriction on resolution prevents IR imaging of many important cell features, a limitation that has driven IR biological studies into the near field.[17] One such emerging method is IR nanospectroscopic absorption imaging[11], which enables chemically specific spectroscopic mapping and label-free chemical identification of materials at the nanoscale[18].

In this paper we illustrate IR nanospectroscopic absorption imaging, often abbreviated as AFM-IR, as a non-destructive tool for intracellular nanoparticle localization. We conjugate GNPs to toluidine blue (TBO) in order confirm IR nanoimaging results with fluorescence microscopy. One of the key advantages of the method, proposed by Dazzi et al[19] is its non-destructive nature which permits analysis of live cells, as it does not require pre-treatment or labeling. By reproduction of FTIR spectra from point sources down to nanoscale resolution[20], AFM-IR has the ability for cellular analysis[21] and intracellular chemical detection.[22] Here we present our results on extension of this application to nanoparticles in cells.

RESULTS

AFM-IR was used to map highly localized gold nanoparticle conjugate densities within cancer cells, and confirm the results with imaging of the nanoparticle conjugated dye (TBO) on a cell by cell basis. We detail simple image analysis methods which confirm the spectral and spatial accuracy of the method upon the sample background, untreated cancer cells and cancer cells containing the TBOGNP molecules. A consistent increase in absorption on the nucleus and cytoplasm was observed in the cells seeded with TBOGNPs relative to a control over a range of incident IR intensities.

TEM was used to characterize the conjugates while uptake was assessed with fluorescence microscopy. A histogram of TBOGNP conjugate diameters (Figure 1a) exhibited a maximum at 5.5 nm. Conjugate diameters were calculated in MATLAB following a pixel to nanometer calibration (see supporting information). Fluorescence microscopy imaging was applied to estimate TBOGNP internalization based on an appropriate choice of fluorescence filters for the TBOGNP emission maxima at 670 nm (Figure 1b). Low density regions of TBOGNPs exhibited

sharp, individual fluorescence emission points in the membrane and cytoplasm where as high density nanoparticles regions were characterized by intense but uneven TBO emission from the cytoplasm and nucleus (Figure 1c). Some fluorescence quenching of the TBO complex was observed as a result of conjugation with the gold nanoparticles. Internal distribution was assessed by co-localization of the nanoparticle emission with nuclei specific DAPI stain in blue (Figure 1d). The DAPI stain also confirmed the characteristic, large nuclei of the cancer cells.

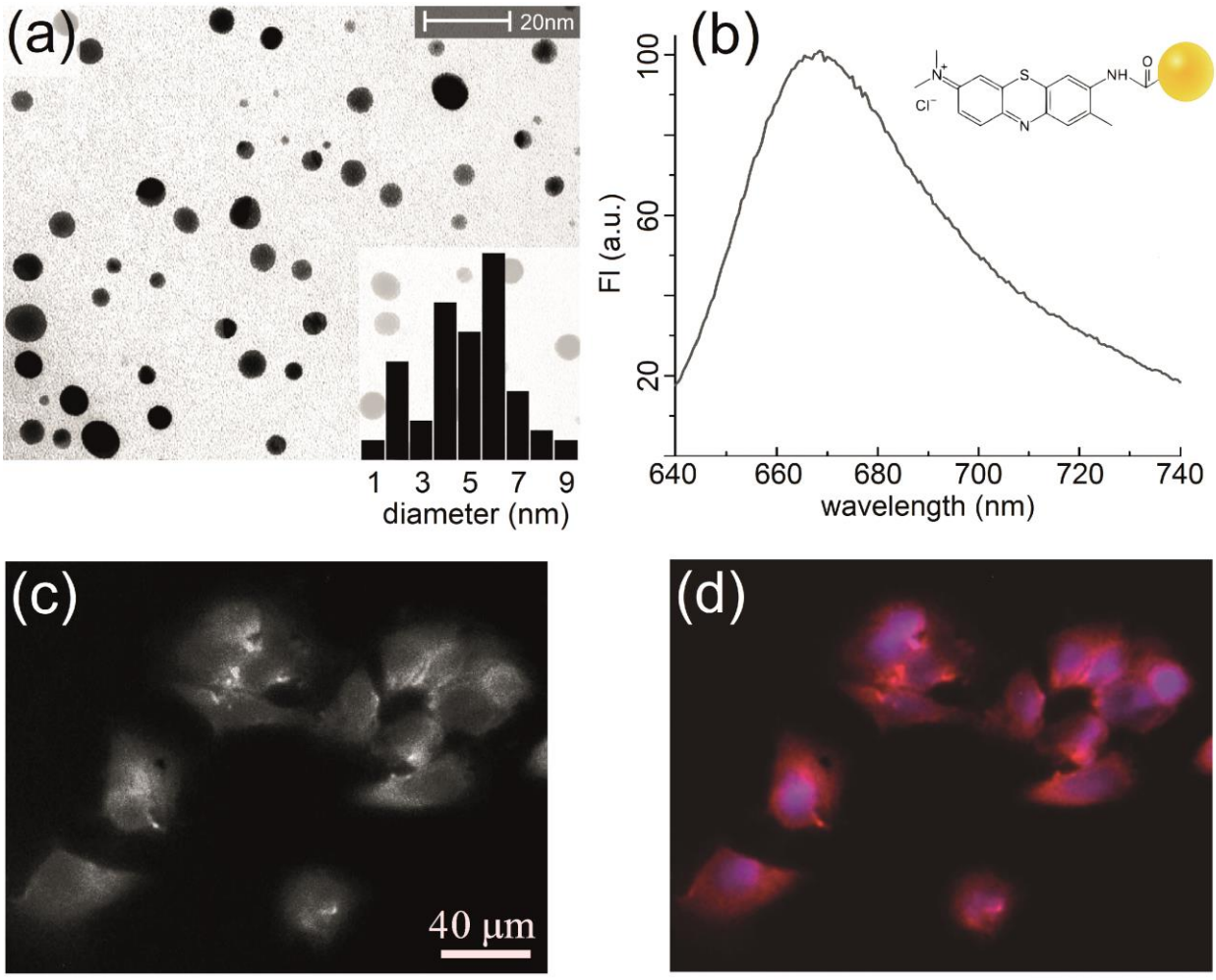

Figure 1 (a) TEM image of the gold nanoparticles conjugated with TBO and a histogram of their diameters (inset), 10 nm scale bar. (b) TBOGNP fluorescence emission showing a 670 nm peak max. The TBOGNP chemical structure is shown in the top right. (c) Fluorescence intensity

from the seeded cells, 20X image filtered for 670 nm emission. Higher intensity is observed from the cytoplasm, although the membrane areas have also accumulated lower levels of TBOGNP (d) Fluorescence colour overlay with TBOGNPs in red and DAPI stain in blue, confirming the characteristic large nuclei of the cancer cells, gamma curve corrected for clarity.

Aside from systemic calibrations, like those performed to account for source intensity variation and laser beam profile, two main experimental areas that require explicit demonstration for true IR nanoimaging; spectral calibration and spatial/volumetric calibration.[23-29] Both need to be addressed in order to detect exogenous agents inside biological media. To confirm the IR spectral response of unseeded cells relative to the substrate background, IR imaging was performed for different absorption bands at the same location. The AFM field of view chosen was 16 μm (Figure 2a), as a full cell view was not practical in terms of the laser intensities required for good signal-to-noise (SNR) with IR nanoimaging using an OPO source (typically on the order of 10^8 W/m^2).[24] Smaller scan areas also permitted faster acquisition times and visualization of finer topographic features, while demonstrating the sub-diffraction limited resolution of the method.

An analysis of the histogram if IR intensities of the typical IR absorption nanoimages shows two peaks in the histogram; a lower sapphire absorption peak and a higher on-cell intensity peak. At different wavelengths, the location of the sapphire intensity peak remains constant because sapphire exhibits constant absorption across the laser's spectral range (see supporting information). An IR image of the AFM region at 2922cm^{-1} excitation is shown in Figure 2b, which exhibits similar features to the topography and membrane perimeters. Two alkane band wavelengths, 2851cm-1 (blue) and 2922cm^{-1} (red) were chosen with different absorption

intensities relative to the constant sapphire background (Figure 2c). Figure 2d shows image histogram of absorption values at each wavelength.

At 2922cm^{-1} excitation (Figure 2d, red) the on-cell peak shifts up from the lower band absorption. In this way, an increase in macroscale FTIR absorption shows good agreement with the increase in nanoscale absorption over a large area of positions. Additionally, by varying excitation wavelength and imaging as above, the relationship between conventional and nanoscale IR spectra can be empirically described. As suggested by theory[27], this relationship is linear, although the chemically complex and spatially heterogeneous nature of the membrane creates local variability in the IR response.

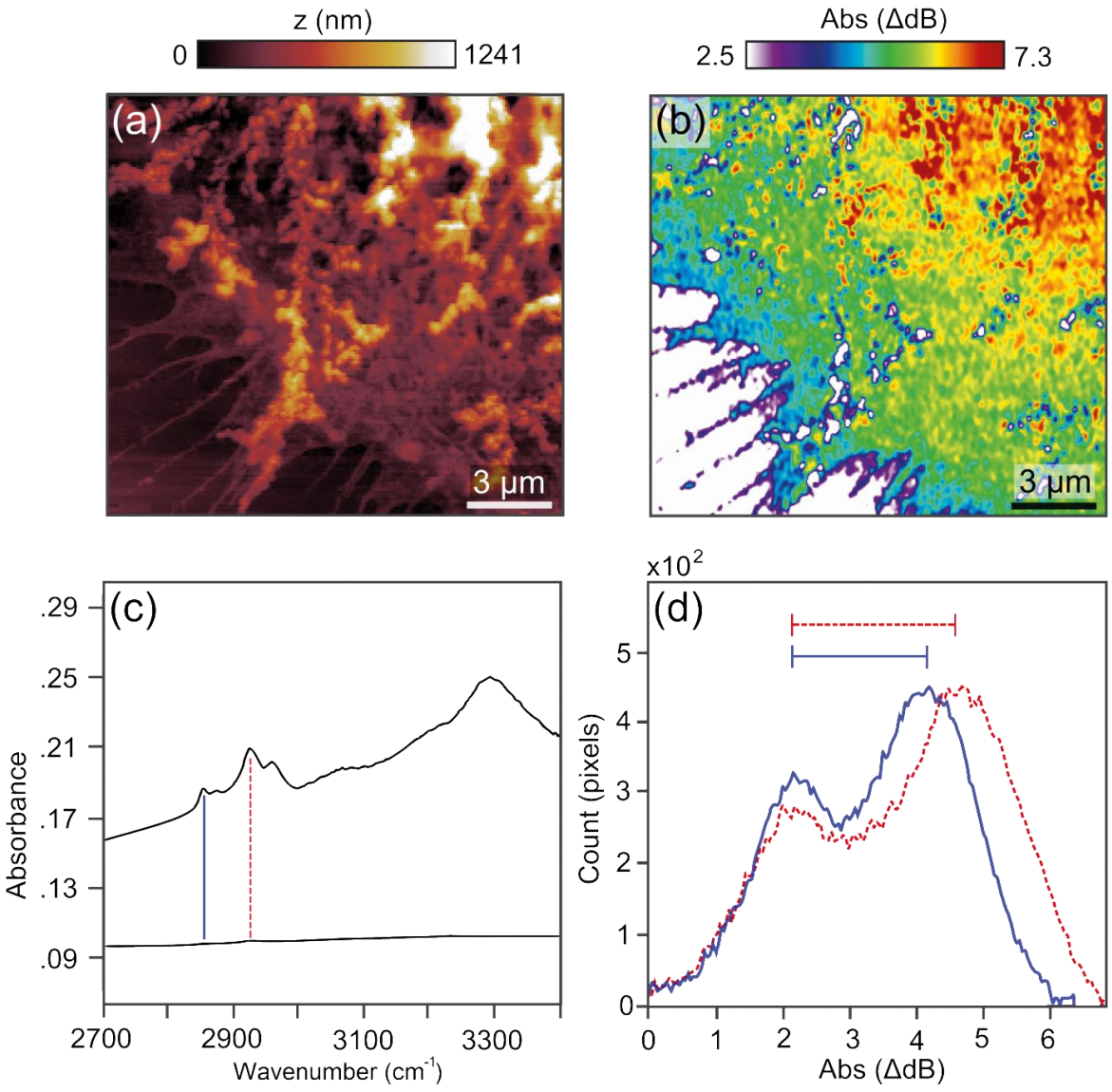

Figure 2 (a) 16μm AFM image subsection of an unseeded cell membrane on the sapphire substrate. (b) The simultaneously recorded IR image of the same region at 2922cm^{-1} excitation, showing close coincidence with the topography and membrane perimeter. (c) FTIR of the sapphire substrate (below) and pure cancer cells (above), with two IR nanoimaging wavelengths illustrated at 2851 cm^{-1} (blue) and 2922 cm^{-1} (red). (d) Two histograms of IR image intensities from the wavelengths illustrated in (c). The lower sapphire peaks, which occur at the same IR

intensity for both wavelengths, have a linear spectrum over this region. The cell absorption peak shifts up 0.65 dB from 2851 cm^{-1} (blue) as a result of increased absorption at 2922 cm^{-1} (red).

Calibration for cell height was necessary for accurate discrimination of the TBOGNP signal, as height can influence the overall absorption intensity, although not the absorption coefficient, at point locations above the cell surface. The cell membranes absorbed several dB above the sapphire substrate, typically from 4-5.5 dB for heights for heights from 300 nm to 1.5 µm, whereas cytoplasmic and nucleic regions showed larger absorption intensities greater than 6 dB with heights primarily ranging from 1.5 to 3.3 µm. This influence was characterized by studies of the spatial change in the absorption profiles of the undoped cancer cells. Previous studies have indicated that the IR absorption signal typically scales with volume.[28] This was confirmed by taking the average AFM-IR absorption response over the range of normal cell heights for wavelengths of interest; two C-H absorption peaks 2851cm^{-1}, 2922 cm^{-1} and a local maxima in the TBOGNP spectrum - 2972cm^{-1} shown in Figure 3.

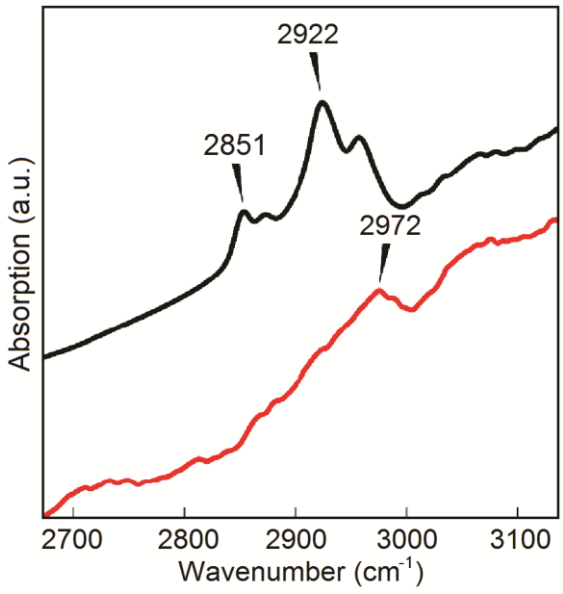

Figure 3 Normalized FTIR absorption of fixed cells (black) and TBOGNP conjugates (red) over the spectral range of interest.

Having defined a quantitative, distribution based method for spectral analysis of IR nanoimages that permits distinction of chemical species within an image (such as sapphire and cells), it was possible to probe the intracellular distribution of TBOGNP with a calibration for the relationship between IR signal and cell height. This was done in tandem with fluorescence microscopy in order to confirm the absorption maps. As fluorescence microscopy and IR nanoimaging provide different orders of spatial resolution, only general features of the nanoimages could be compared.

An example of this is given in Figure 4a, which shows 670 nm fluorescent emission for localization of TBOGNPs to the cytoplasm and nucleus. This permitted a choice of AFM scan region where TBOGNP presence was clearly indicated in a subsection of the fluorescence image (white box). The ratio of absorption at 2972cm^{-1} to 2922cm^{-1} was recorded at each point within the subsection, shown in Figure 4b. AFM-IR ratio imaging has previously demonstrated nanoscale distinction and phase assessment of pharmaceutical blends[28]. The specific ratio here was chosen because regions containing TBOGNP should exhibit a ratio value greater than one, and regions containing cells but no nanoparticles should have a value less than 1 based on the extension to the nanoscale of the cell and TBOGNP FTIR spectra in Figure 3. Sapphire areas, which absorb equally at each wavelength, would remain close to unity, since the absorption intensity remains the same for different excitation wavelengths. The numerical range of such a ratio image depends on the definition of what constitutes an absorption value of zero, which depends on the SNR of the AFM-IR device and is therefore system specific.

In the IR ratio image, substrate regions are close to unity (colour-coded green) because both wavelengths are absorbed equally by sapphire (T=78%). The membrane displays an absorption increase due to the presence of TBOGNP, but is offset by the reduction in cell absorption from 2922-2972 cm^{-1}. Regions of no TBOGNP are less than one as pure cells see an absorption reduction for this ratio. Significant red channel intensity for this wavelength ratio, and thus TBOGNP presence, is only evident inside the cytoplasm, which is confirmed by fluorescence emission co-localization in Figure 4a. Membrane regions also showed sub-micron sized pockets of high (1.05 to 1.15) and low (0.8 to 0.9) particle density, although due to their size, these were not co-localizable with fluorescence microscopy, and may indicate a more complex local density distribution than was possible with conventional microscopy. Similarly, previous near-field IR studies have permitted chemical distinction at spatial resolutions down to 100 DNA molecules[30].

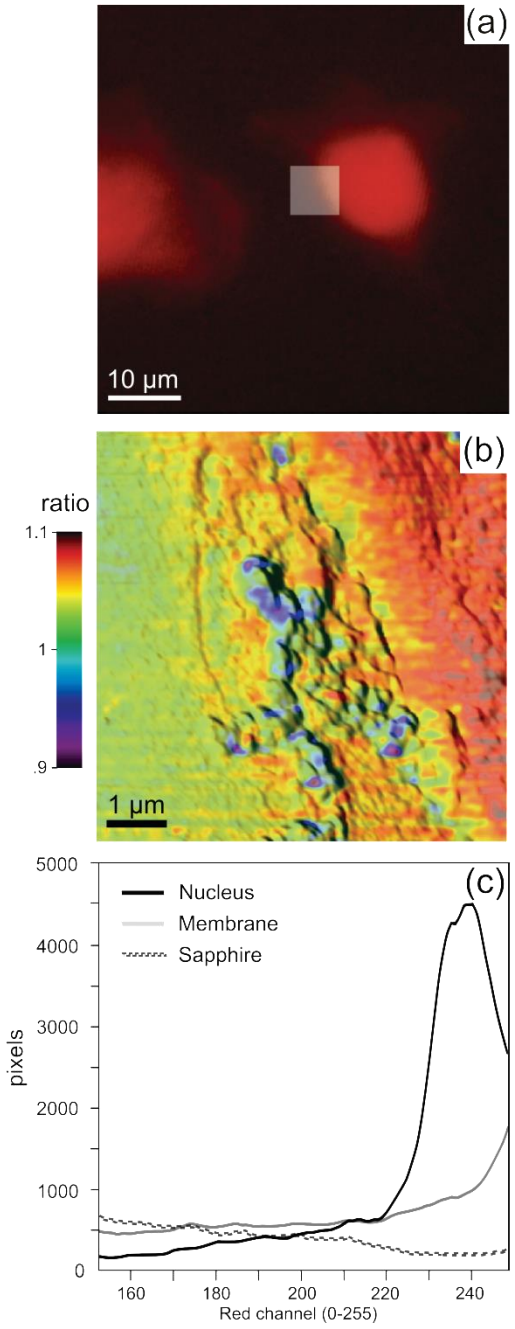

Figure 4 (a) Fluorescence microscopy showing diffraction limited TBOGNP localization indicating the 6.5 µm subsection used for AFM-IR imaging (box inset). b) Topography/IR absorption ratio overlay, scale bar: 1 µm. c) Red channel intensity ranges from (b) for the sapphire background (dotted line), membrane (grey line) and cytoplasm and nucleus (black line).

Significant red channel intensity for this wavelength ratio, and thus TBOGNP presence, is only evident in the cytoplasm, which is confirmed by fluorescence emission co-localization in (a).

In the colour coding used for the IR ratio image, red indicates nanoparticle presence, as in the fluorescence image. However, the nanoimaging method is not diffraction limited and can achieve similar results, but with a much higher resolution, limited only by the AFM tip apex dimensions and not thermal effects.[18] In Figure 4c, by observation of the red channel intensity ranges for the sapphire background (dotted line), membrane (grey line) and cytoplasm and nucleus (black line), a simple image analysis method is suggested for localizing TBOGNPs within cells. Significant channel intensity for this wavelength ratio is only evident in from the cytoplasm red channel, a result which is confirmed by fluorescence microscopy in Figure 4a. The large cytoplasm red channel peak from 230 to 240 pixel value indicates TBOGNPs for this configuration, a peak not seen in the membrane or sapphire areas.

The red channel intensity, indicating an increase in absorption in the vicinity of high density TBOGNP can be contributed to several phenomena. At these wavelengths, the TBOGNP signal cumulatively adds to that of the cells such that signal ratio of the wavelengths 2972-2922 cm^{-1} should increase in the presence of TBOGNP. Secondly, the gold nanoparticles increase the local internal scattering of light, which increases the effective photon path length inside the cells where TBOGNP is present; this artificially increases the cell absorption. Enhancement of the signal by nanoparticles also occurs and is a previously observed phenomena[6]. However the extent of the signal increase is surprising given that pure cells actually absorb a few percent less at 2972cm^{-1}.

DISCUSSION

Figure 4b contains resolvable IR hotspots and chemical features below 300nm. The resolution of each pixel is defined by the tip-sample geometry, which by our estimate, indicates a lateral resolution below 50 nm. In contrast, were this image taken with a perfect far field IR imaging system at the same excitations, the resolution would be approximately 1.7 μm/pixel – which would make this ratio map less resolved than a 5 pixel grid. Therefore AFM-IR has permitted spectrally specific localization of the TBOGNP conjugates in cells at ≈λ/70 nm, far below the diffraction limit. However, AFM-IR is capable of even higher lateral resolution[20].

Although this method permits whole image chemical mapping at high resolution, it has some limitations. The absorption SNR and the co-averaged sampling rate, which are interdependent properties, limited the pixel readout speed to 10 to 30 Hz depending on laser stability. Although slow, this was necessary in these experiments to ensure meaningful spectral detail given the low particle density of the TBOGNP conjugation when considered relative to the cell volume. Such acquisition speeds mean that a 5 μm^2 image at high resolution (50nm per pixel) can easily take 6 minutes to collect at a rate of 0.3 Hz per line, even neglecting the time lost to masked lines at the image boundaries which are necessary for robust AFM – IR image pixel overlapping. Additionally, the acquisition of such IR nanoimages is not without effort given the effects of sample thermal drift for acquisition times of this length and greater.

High speed AFM-IR will be possible with the use of smaller, higher frequency cantilevers which will have a faster relaxation time, combined with IR sources of a higher pulse repetition rate. However, the extent of cantilever deflection to a set surface expansion, which is a direct measure of the absorption SNR, is inversely proportional to the frequency of cantilever

resonance and its mass. In response to this dual set of limitations, novel probe designs have been suggested to minimize cantilever mass and improve the methods absorption sensitivity.[31] Further research into optimized sources, such as top-down fiber guided excitation and AFM-IR specific probes could increase the ease and speed of AFM-IR imaging, allowing the observation of time-dependent subcellular chemical processes at nanoscale resolutions.

An immediate alternative to such systemic improvements is to avoid full IR imaging, instead taking the IR spectra, and thus chemical information, from point sources on the cell surface. This provides an excellent alterative to full multi-wavelength chemical maps as it reduces the acquisition time by a factor of 10^4 compared to standard imaging, allowing for feasible distribution studies not just images of cell subsections, but of multiple whole cells. We demonstrate this alternative by taking the IR signal from point sources of 70 cells, including both a control and a separate TBOGNP-seeded culture. The cytoplasmic absorption of each cell was obtained over a range of laser intensities (3.5 to 4.5 mW) in order to rule out any nonlinearity in the laser intensity influence on absorption (Figure 5). Were this study performed on an individual cell, it would be statistically less viable, as an individual cell may have atypical properties, such as highly uneven TBOGNP uptake and distribution.

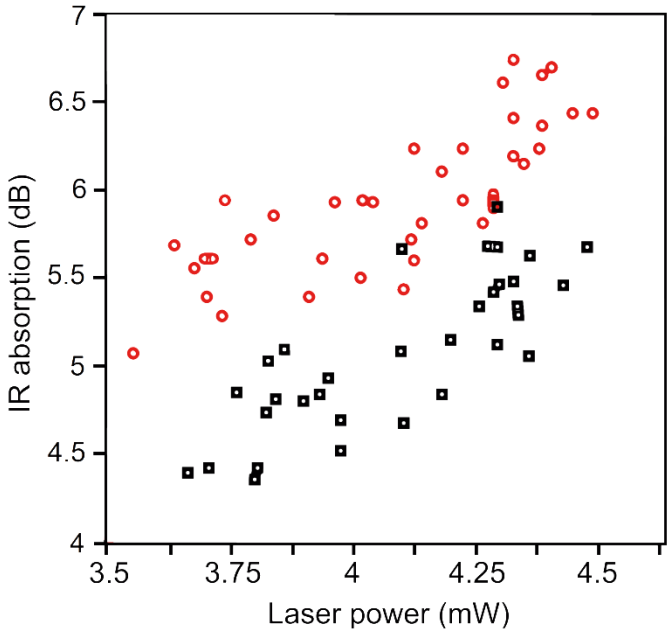

Figure 5. AFM-IR absorption values in decibels for pure cells (black) and cells containing TBOGNP (red) over a range of laser intensities. Different centrally defined (see supporting information) positions were chosen at 2922 cm^{-1} excitation over a range of laser intensities. A consistent distinction of 0.95 dB is seen between the seeded cells and the control group. Acquisition time including averaging for each IR reading was below 300 ms. The anticipated 2 standard deviation signal variation is shown in grey.

Centrally defined positions on the cells were chosen where DAPI stain was prevalent. An acquisition averaging time of 300 ms was defined per data point. Because the sample stage could be moved without altering the OPO laser-cantilever tip alignment, changing cell did not require any realignment processes. This meant that retracting and replacing the tip on to a stained position of a cell was the only process required after each absorption reading. A graph of absorption intensity against laser power for pure cells (black) and cells containing TBOGNP (red) is shown in Figure 5. The excitation was kept constant at 2922cm^{-1} over the range of laser intensities. A consistent increase of 0.95 dB is seen on the seeded cells compared to the control

group. This indicates TBOGNP presence for two reasons: first, the IR absorption of TBOGNPs is cumulatively adds to that of the cells; second, the gold nanoparticles enhance the internal scattering of light, which increases the effective photon path length inside the cells. The anticipated signal variation for our level of laser stability for this acquisition time is shown in grey.

Therefore, using of IR point sources lets us extend the AFM-IR technique from subcellular analysis up to studies of cell numbers that are statistically significant. We present these as complementary techniques and, although such other techniques as flow cytometry are more effective for distribution studies, this method can be used without having to treat or destroy the sample in a separate characterisation experiment. It also permits detailed IR nanoimages of a specific cell to be seen in the context of the cell's position in an overall distribution.

CONCLUSION

Intense research into the application of non-destructive near field imaging methods has primarily been driven by the promise of chemical distinction on the nanoscale. Infrared spectroscopy is a robust and longstanding method for data extraction from multiple heterogeneous chemical signatures. The magnitude and scope of this prior research in IR spectroscopy provides an immediate advantage to its extension to the nanoscale when compared to nanospectroscopic methods which, due to the novelty of the acquisition method, cannot rely on a large catalogue of previous experiments and a standardized method such as FTIR for confirmation. We illustrate a key example of this advantage by verifying that IR nanospectral absorption imaging is capable of nanoparticle localization in biological systems using the example of metallic nanoparticle-TBO conjugates within colon adenocarcinoma cells. These

studies demonstrate that AFM-IR is a viable tool for high resolution subcellular particle detection without the need for pre-treatment of the sample.

As this method is chemically specific, the natural progression of this work is the extension of its application to materials which cannot be easily fluorescently labelled within live cells. Further to this, IR spectral ratio imaging was performed in order to explore the subcellular spatial distribution of the nanoparticles, which suggested complex local TBOGNP densities below the resolvable limits of fluorescence microscopy. Additionally, point source nanospectroscopy permitted distinction of nanoparticle seeded cells from a control group with 95% confidence, illustrating IR nanoimaging as a highly effective, yet non-invasive method for localizing nanoparticles at sub-diffraction limited resolution within biological systems.

Materials and Methods

TBOGNPs were synthesized using Sigma Aldrich (St. Louis, USA) materials and millipure water used throughout. Concentration values for the TBOGNP conjugates describing the concentration of the TBOs on the gold surface were determined by absorption spectroscopy. Visible spectroscopy of the TBOGNP conjugates was performed in order to assess the nanoparticles' fluorescent emission peak using a UV-Vis spectrometer (Varian, UK, Coventry). The conjugates' sizes were determined by transmission electron microscopy via evaporation on a carbon coated copper grid. The infrared spectrum of TBOGNPs was recorded with a FTIR spectrometer (Agilent, Santa Clara, CA).

Culture

Sapphire windows were chosen as substrates for the cells due to their linear, low absorption response in the IR region of interest. The substrates were sterilized by autoclaving and placed into a 6 well plate. A human colon adenocarcinoma cell line (SW480) at a concentration of 10^6 cells/ml was seeded in the wells with 2 ml DMEM medium and incubated at 37° C in a 5% CO2 for 24 hours. The cells were then incubated with TBOGNPs at 816 μM conc. in the dark for 12 hours after which the wells were rinsed at least three times with phosphate buffered saline (PBS) to remove the nanoparticle conjugates that had not been internalised by the cells. The cells were then fixed with 3.7% paraformaldehyde for 10 minutes. Cell viability was unaffected by TBOGNP internalization at this concentration. Cell spectra were recorded with a FTIR spectrometer (Agilent, Santa Clara, CA) by subtracting the spectra obtained of the substrate held by a custom mount at the beam focus from the spectra obtained of the fixed cells.

AFM-IR methodology

The AFM-IR experimental setup is shown in Figure 6, the methodology has been described elsewhere.[22-28] Briefly, when incident pulses were tuned to a vibrational resonance of the cells or TBOGNPs the infrared light absorbed was proportional to the materials' absorption coefficients at the excitation wavelength, causing thermal heating which relaxed mechanically via expansion of the surface.[23] This deformation of the surface causes deflection of the mechanical probe in contact mode, which relaxes back according to a one end fixed-cantilever solution to the Euler-Bernoulli equation. The cantilever deflection is measured independently of the atomic force microscope (AFM) feedback, as the tip oscillation decays in under a 10^{th} of the topographical sampling period. Taking the Fourier Transform (FT) of the cantilever relaxation indicated a single strong peak with a frequency specific to the tip used. Absorption maps were produced by

iteratively sampling the intensity of this peak at 128 pulse coaveraging during acquisition of the topography.

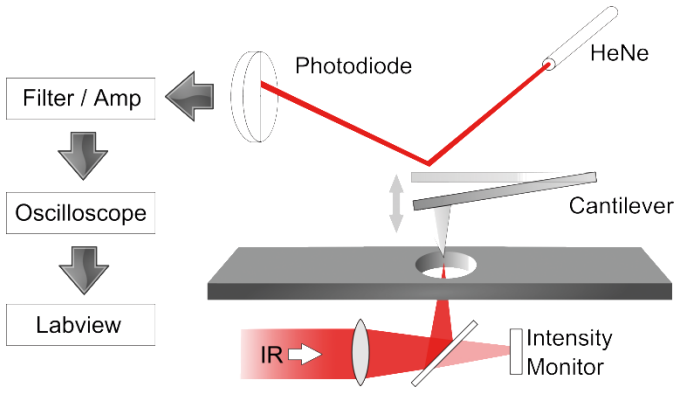

Figure 6 - The experimental setup. IR pulses are directed up to the AFM tip apex. The resulting signal is filtered and amplified and then iteratively read out over the scan area.

An optical parametric oscillator laser was used as the IR light source with continuous spectral output from 3231–4200 nm in pulsed (ns) mode operation at a 2 KHz repetition rate. The pulses were focused by an IR lens and split with a CaF2 beam splitter (Edmund Optics, USA Barrington, NJ) into a PbSe Fixed Gain IR Detector (Thorlabs, UK, Ely). The monitor intensity was averaged every 32 milliseconds which allowed continual calibration of the light source. The pulses were directed to the AFM tip apex using a gimbal mounted mirror. This allowed the sample stage to be moved without altering the OPO laser-cantilever tip alignment - this also precluded sample position from any realignment processes.

CONFLICT OF INTEREST

The authors declare no competing financial interest

ACKNOWLEDGEMENTS

Work in the UCD nanophotonics team is primarily funded by the Irish Research Council (IRC) with equipment used in this work funded by Science Foundation Ireland (SFI). This research was co-funded by the Islamic development bank and the Ministry of Higher Education and Scientific Research of Iraq. The authors would like to thank Dermot Keenan for his assistance with infrared spectroscopy of cells.

SUPPORTING INFORMATION AVAILABLE

Additional figures, supplementary text and the code for image processing is available including details of nanoparticle sizing from TEM. Full spectra from the substrate, cells and TBOGNP complex are presented and compared to the literature. The choice of IR image coloring and contrast are explained including discussion of the IR image background. For completeness, IR nanospectroscopy and imaging of isolated TBOGNP aggregates are presented.

REFERENCES

[1] Jain P. K.; El-Sayed I. H.; El-Sayed M. A.; Au nanoparticles target cancer *Nano Today* **2007**, *1*, 18-29

[2] Albanese A.; Tang P. S.; Chan C.W. The effect of nanoparticle size, shape, and surface chemistry on biological systems. *Annu. Rev. Biomed. Eng*. **2012**, *14*, 1-16

[3] Trono J. D.; Mizuno K.; Yusa N.; Matsukawa T.; Yokoyama K.; Uesaka M. Size, concentration and incubation time dependence of gold nanoparticle uptake into pancreas cancer cells and its future application to X-Ray Drug Delivery System. *Radiat Res.* **2011**, *52*, 103-109

[4] Murphy C. J.; Stone J. W.; Sisco P. N.; Alkilany A. M.; Goldsmith E.C.; Baxter S. C. Gold Nanoparticles in Biology: Beyond Toxicity to Cellular Imaging *Acc. Chem. Res.* 2008, *41*, 1721-1730

[5] Hong H.; Zhang Y.; Sun J.; Cai W.; Molecular imaging and therapy of cancer with radiolabeled nanoparticles. *Nano Today* **2009,** *4*, 399-413

[6] T. G. Iversen, T. Skotland, K. Sandvig Endocytosis and intracellular transport of nanoparticles: Present knowledge and the need for future studies. *Nano Today* **2011**, *6*, 176-185

[7] Qian W.; Huang X.; Kang B.; El-Sayed M. A. Dark-field light scattering imaging of living cancer cell component from birth through division using bioconjugated gold nanoprobes. *J Biomed Opt*. **2010**, *15*, 046025.

[8] Morones J. R.; Yacaman M. J. et al. The bacterial effect of silver nanoparticles *Nanotechnol*. **2005**, *16*, 2346–2353

[9] Hajibagheri M. A. N. Electron Microscopy: Methods and Protocols *Meth. in Mol. Biol.* **2007**, *117*, 1

[10] Dufrene Y. F.; Garcia-Parajo M. F. Recent progress in cell surface nanoscopy: Light and force in the near-field *Nano Today* **2012**, *7*, 390-403

[11] Dazzi A.; Prazeres R.; Glotin F.; Ortega J.M. Analysis of nano-chemical mapping performed by an AFM-based ("AFMIR") acousto-optic technique. *Ultramicroscopy*, **2007**, *107*, 1194-1200

[12] Nann T. Nanoparticles in photodynamic therapy. *Nano Biomed. Eng.* **2011**, *3*, 137-143

[13] Willig K. I.; Harke B.; Medda R.; Hell S. W.; STED microscopy with continuous wave beams *Nat. Methods* **2007**, *4*, 915 - 918

[14] Wood B. R.; Ashgari-Khiavi M.; Bailo E.; McNaughton D.; Deckert V.; Detection of nano-oxidation sites on the surface of hemoglobin crystals using Tip-Enhanced Raman Scattering. *Nanolett.* **2012**, *12*, 1555-1560

[15] Parekh S. H.; Lee Y. J.; Aamer K. A.; Cicerone M. T.; Label-free cellular imaging by broadband coherent anti-Stokes Raman scattering microscopy. *Biophys J*. **2010**, *8*, 2695-704.

[16] R. Bhargava. Infrared Spectroscopic Imaging: The Next Generation. *App. Spec.* **2012**, *66*, 1091-1120

[17] Hinterdofer P.; Garcia-Parajo M. F.; Dufrene Y. F. Single-molecule imaging of cell surfaces using near-field nanoscopy. *Acc. Chem. Res.* **2012**, *45*, 327-336

[18] Felts J. R.; Kjoller K.; Lo M.; Prater C. B.; King W. P. Nanometer-Scale Infrared Spectroscopy of Heterogeneous Polymer Nanostructures Fabricated by Tip-Based Nanofabrication *ACS Nano* **2012**, *6*, 8015–802

[19] Dazzi A.; Prazeres R.; Glotin F.; Ortega J. M. Subwavelength infrared spectromicroscopy using an AFM as a local absorption sensor. *Infr. Phys. & Tech.* **2006**, *49*, 113-121

[20] Mayet C.; Deniset-Besseau A.; Prazeres R.; Ortega J.M.; Dazzi A. Analysis of bacterial polyhydroxybutyrate production by multimodal nanoimaging. *Biotechnol Adv.* **2012** PMID: 22634017

[21] Mayet C.; Dazzi A.; Prazeres R.; Allot F.; Glotin F.; Ortega J. M. Sub-100 nm IR spectromicroscopy of living cells. *Opt. Lett.* **2008**, *33*, 1611-1613

[22] Mayet C.; Dazzi A.; Prazeres R.; Ortega J. M.; Jaillard D. In situ identification and imaging of bacterial polymer nanogranules by infrared nanospectroscopy. *Analyst*, **2010**, *135*, 2540-2545

[23] Yarrow F.; Kennedy E.; Salaun F.; Rice J. H. Sub-wavelength infrared imaging of lipids. *Biomed. Opt. Express* **2011**, *2*, 37–43

[24] Kennedy E.; Yarrow F.; Rice J. H. Nanoscale spectroscopy and imaging of hemoglobin *J. Biophot*. **2011,** *4*, 588–591

[25] Rice J. H.; Far-field fluorescence microscopy beyond the diffraction limit: Fluorescence imaging with ultrahigh resolution *Molecular Biosystems* **2007**, *3*, 781-793

[26] Rice J. H., Nanoscale optical imaging by atomic force infrared microscopy *Nanoscale* **2010**, *5*, 660-667

[27] Yarrow F.; Rice J. H.; Localized IR spectroscopy of hemoglobin. *Eur Biophys J.* **2011**, *40*, 217-219

[28] Dazzi A.; Glotin F.; Carminati R. Theory of infrared nanospectroscopy by photothermal induced resonance. *J. Appl. Phys* **2010**, *107*, 124519-124527

[29] Van Eerdenbrugh b.; Lo M.; Kjoller K.; Marcott C.; Taylor L. S.; Nanoscale mid-infrared imaging of phase separation in a drug–polymer blend. *J Pharm Sci* **2012**, *101*, 2066-2073

[30] Kopf I.; Grunwald C.; Brundermann E.; Casalis L.; Scoles G.; Havenith M. Detection of hybridization on nanografted oligonucleotides using scanning near-field infrared microscopy. *J. Phys. Chem* **2010**, *114*, 1306–1311

[31] Kjoller K.; Felts J. R.; Cook D.; Prater C. B.; King W. P. High-sensitivity nanometer-scale infrared spectroscopy using a contact mode microcantilever with an internal resonator paddle. *Nanotechnology* **2010,** *21,* 185705.